J Mater Sci (2018) 53:13364–13379

Mechanochemical Synthesis

Phase formation under non-equilibrium processing conditions: rapid solidification processing and mechanical alloying

C. Suryanarayana[1,*]

[1] Department of Mechanical and Aerospace Engineering, University of Central Florida, Orlando, FL 32816-2450, USA

Received: 18 January 2018
Accepted: 2 March 2018
Published online: 9 March 2018

ABSTRACT

Rapid solidification processing (RSP) of metallic alloys, involving solidification of liquid metals at very high rates, results in the formation of a variety of metastable phases such as supersaturated solid solutions, crystalline intermetallic compounds, quasicrystalline phases, and metallic glasses. Additionally, significant refinement of the grain sizes and segregation patterns also occurs. Mechanical alloying (MA), another powerful non-equilibrium processing technique, utilizes repeated cold welding, fracturing, and rewelding of powder particles in a high-energy ball mill. MA also results in the formation of metastable phases and microstructural refinement similar to what happens during RSP. Consequently, comparisons are frequently made between the phases produced by RSP and MA and the general understanding is that they both result in similar metastable effects. A detailed analysis of the metastable phases produced by RSP and MA is made in the present work, and it is shown that even though the effects may appear similar, the mechanisms of formation and the composition ranges in which particular phases form are quite different. These two methods also have some unique features and produce different phases. The differences have been ascribed to the fact that RSP involves solidification from the melt while MA is a completely solid-state process that is not restricted by the phase diagram.

Introduction

A number of novel and advanced materials have been developed during the last 50 years or so using different non-equilibrium processing methods [1]. These include metallic glasses [2, 3] (including the relatively recently developed bulk metallic glasses [4]), quasicrystals [5, 6], high-temperature superconductors, superhard carbonitrides, diamond-like carbon thin-films, and nanostructured materials [7–9]. Several new techniques have been developed for the processing and characterization of metastable materials. A common feature of the methods used to obtain these advanced materials has been to carry out

Address correspondence to E-mail: Surya@ucf.edu

https://doi.org/10.1007/s10853-018-2197-4

processing under far-from-equilibrium conditions; thus, the materials developed are usually in a metastable or non-equilibrium state. Turnbull [10] coined the phrase "energize and quench" to describe these processes and these materials are also referred to as "driven alloys" [11]. It is through such processes that the constitution and microstructure of materials can be drastically altered to achieve beneficial properties. The available non-equilibrium processing techniques include rapid solidification processing (RSP) from the melt, mechanical alloying (MA), laser processing, plasma processing, spray forming, physical and chemical vapor deposition techniques, and ion mixing. The principles and relative advantages and disadvantages of these techniques have been discussed in the literature (see, for example, Ref. [1]).

Even though the number of non-equilibrium processing methods is large, RSP and MA have been the most commonly used methods by far. A very large amount of data have been generated on the synthesis and characterization of different metastable phases using these two processing techniques. The metastable phases prepared include supersaturated solid solutions, metastable intermetallic phases, quasicrystals, and metallic glasses. It has often been pointed out in the literature that the results obtained by the RSP and MA techniques are very similar in any alloy system. The main goal of the analysis presented in this paper is to show that even though there are many apparent similarities, there are also significant differences in the types of phases produced, the composition ranges in which these phases could be synthesized, and the microstructures of the products. Additionally, contamination of the powder during MA appears to play an important role in deciding the nature of the phase produced and the composition range in which it is synthesized.

Before discussing the similarities and differences between the products obtained by RSP and MA methods, let us briefly describe the salient features of the techniques and their main attributes.

Rapid solidification processing

The technique of rapid solidification processing (RSP) was developed by Pol Duwez in 1960 in response to an academic curiosity. Concerned with the non-systematic behavior of the Cu–Au, Ag–Au, and Cu–Ag alloys in following the Hume–Rothery rules for the formation of substitutional solid solutions, and in particular noting that the Cu–Ag system did not exhibit the expected isomorphous behavior under equilibrium conditions, Duwez decided to subject the molten Cu–Ag alloys to solidification at very high cooling rates of about 10^6 K/s. X-ray diffraction patterns of these rapidly quenched alloys clearly showed that a continuous series of solid solutions was obtained in the whole composition range of the alloy system [12]. This interesting result was followed, in the same year, by the observation of a missing Hume–Rothery compound in the Ag–Ge system [13], and most dramatically through observation of a metallic glassy structure in the Au–Si system [14]. Duwez summarized the various capabilities of this technique later [15].

The most important requirement for obtaining metastable phases through RSP is the significant undercooling achieved in the melt before solidification occurs; this has been achieved through imposition of high solidification rates. Such high cooling rates have been obtained by (1) allowing molten droplets to solidify either in the form of splats on a good thermally conducting substrate (e.g., in ''gun'' quenching), or by impinging a cold stream of air or an inert gas against the molten droplets (e.g., in atomization), or (2) stabilizing a flowing melt stream so that it freezes as a continuous filament, ribbon, or sheet in contact with a moving chill surface (melt spinning and its variants), or (3) surface melting technologies involving rapid melting at a surface followed by fast cooling sustained by rapid heat extraction into the unmelted block (laser surface treatments). Various techniques based on these three categories have been developed over the years, as summarized previously [16, 17]. By a judicious choice of the alloy system and composition, it has been possible, during the last 25 years or so, to decrease the critical cooling rates for glass formation to less than about 10^2 K/s and thereby substantially increasing the section thickness of metallic glasses. These alloys, known as bulk metallic glasses, have now reached a diameter of 80 mm [18] and find a number of applications [4, 19].

In addition to the constitutional changes listed above, ultrafine microstructures commonly down to micrometer dimensions, but occasionally to nanometer levels, and refined segregation patterns have been observed in alloys solidified at such high rates. Rapidly solidified materials have been finding

a multitude of applications, including soft (for transformer core laminations) and hard magnetic materials, wear-resistant light alloys, materials with enhanced catalytic performance and applications in fuel cells, tool steels, and superalloys consolidated by powder metallurgy methods, and new alloys for medical implants and dental amalgams [20].

The benefits of RSP can be summarized as follows:

1. Formation of supersaturated solid solutions.
2. Synthesis of metastable intermetallic phases, including quasicrystalline phases.
3. Production of metallic glasses.
4. Refinement of grain sizes and segregation patterns.

Mechanical alloying

Mechanical alloying (MA) was developed by John Benjamin in 1966 at the INCO laboratories, out of an industrial necessity, to produce oxide-dispersion-strengthened Ni-based superalloys for gas turbine applications that combined the high-temperature strength of oxide dispersion and the intermediate temperature strength of γ' precipitate [21]. Subsequently, it was shown that this technique was also capable of synthesizing a variety of metastable phases including supersaturated solid solutions, non-equilibrium intermetallic phases, quasicrystalline phases, and amorphous solids.

The process of MA is based on repeated cold welding, fracturing, and rewelding of powder particles in a high-energy ball mill. An appropriate amount of powder mixture and grinding medium (usually made of steel or tungsten carbide) is loaded into the milling container and milled for the desired length of time. Typically, a ball-to-powder weight ratio of 10:1 or higher is used. The repeated severe plastic deformation experienced by the powder particles results in a lamellar structure if soft and ductile materials are processed or in an intimate mixture of the constituent powders, if brittle materials are involved. Additionally, a high density of crystal defects (grain boundaries, dislocations, stacking faults, vacancies) is introduced. The powder temperature rises slightly due to the mechanical energy dissipated during collisions. The grain refinement and mechanical mixing, enhanced diffusivity due to presence of short-circuit diffusion paths, reduced diffusion distances, and slight rise in temperature allow alloying to occur. Accordingly, by a proper choice of the process parameters and suitable alloy composition, it is possible to produce various alloy phases.

A process control agent (PCA) may be added when ductile powders are milled to prevent or reduce excessive agglomeration of the powder and sticking of the powder to the grinding media and the container walls. Powder contamination is a serious concern. It can originate from (1) evaporation of the PCA during milling and incorporation of its constituents into the powder, (2) wear and tear of the milling media, and (3) the atmosphere under which the powder is milled. On the other hand, MA exhibits some unique features such as (1) formation of alloys at near ambient temperatures, (2) ability to alloy (and even form amorphous phases) between metals with positive heats of mixing, and (3) uniform dispersion of a large volume fraction of fine second-phase particles in metallic matrices [22]. MA has also been used to produce nanostructured monolithic and composite materials and alloys from immiscible elements. Additionally, chemical reactions could be initiated to produce novel materials and pure metals from their ores. Details of the process, mechanism of alloying, phase formation, and their applications have been summarized in the literature [23–26].

The benefits of MA can be summarized as:

1. Production of fine dispersion of second-phase particles.
2. Refinement of grain sizes, frequently down to nanometer levels.
3. Formation of metastable phases (solid solutions, intermetallic phases, quasicrystalline phases, and amorphous alloys).
4. Inducement of mechanochemical reactions.
5. Alloying of difficult-to-alloy elements.
6. Easy scale-up to commercial quantities.

From the above, it is very clear that the non-equilibrium effects achieved by RSP have also been observed in MA powders. Therefore, comparisons are frequently made to determine the efficiencies of these two techniques in producing metastable phases and also to determine whether there are any differences between the products of the two methods. It is, however, important to realize that while both RSP and MA are non-equilibrium processing methods producing a variety of similar metastable phases and

microstructural modifications, RSP requires that the alloy is melted and then solidified rapidly, while MA is a completely solid-state processing method. Since no melting is involved in the MA process (unless very low melting-point metals are milled), phase diagram restrictions do not apply in this case. Therefore, any powder mixture can be processed by MA and the preparations of alloys that are not available for RSP are often possible.

Let us now discuss the similarities and differences in the metastable phases produced by the RSP and MA methods.

Solid solutions

According to the Hume–Rothery rules, two elements can form a substitutional solid solution if (1) their atomic radii differ by less than about ± 15%, (2) their electronegativities are close, (3) they have the same crystal structure, and (4) similar valences. In spite of satisfying all these conditions, the Ag–Cu system, among others, does not exhibit the expected isomorphous behavior, but decomposes according to a eutectic reaction. However, the initial experiments of Duwez have convincingly proved that rapid solidification of molten alloys in this system results in the formation of a continuous series of solid solutions [12]. Subsequently, a few other systems that deviate from the Hume–Rothery rules were also shown to behave in a similar manner. In other systems, where it was not possible to achieve complete solid solubility of the two elements, large extensions of solid solubility limits were reported [24, 27]. In the early years of research on RSP, it was suggested that the maximum solid solubility levels achieved are determined by the nature of the phase diagrams. For example, the maximum solid solubility limit is limited by the equilibrium solid solubility at the eutectic or peritectic temperatures. This is because, beyond this limit, the second phase starts nucleating and prevents further extension of solid solubility limit. This was, however, not borne out by many investigations. This is understandable because phase diagram show the equilibrium behavior dictated by thermodynamics, while the constitution of the RSP product is mainly determined by kinetic factors. In fact, there are more exceptions to this statement than instances when it was followed. Based on a large number of solid solubility extensions observed in a number of alloy systems, it was reported that the solid solubility extension was significantly higher if the equilibrium solid solubility was very small [28].

Solid solutions (both equilibrium and extended) were also reported to form in mechanically alloyed powders. For example, complete mutual solid solubility of Cu and Ag was reported by Uenishi et al. [29]. Figure 1 shows a plot of the lattice parameter of the solid solution phase obtained by MA and RSP techniques as a function of the Ag content in the Cu–Ag system. The lattice parameters for the MA powders were taken from Ref. [29] and those for RSP alloys from Ref. [30]. The behavior is very similar in both the cases. Large solid solubility extensions by MA were also reported in a number of alloy systems, listed in Refs. [23, 24]. Table 1 presents some typical solid solubility-level extensions achieved in RSP and MA alloys.

The solid solubility limits obtained by MA appear to be determined by conditions different from those listed for RSP alloys. For example, the largest extension in solid solubility in MA powders will be obtained before the onset of amorphization. Another observation was that the solid solubility is higher if the solvent grain size is very small, typically in the nanometer dimensions [31, 32]. (It is possible that the solute atoms segregate to grain boundaries because of the vastly increased grain boundary area.) Another approach suggested that the solubility limit is determined by a balance between intermixing due to shear

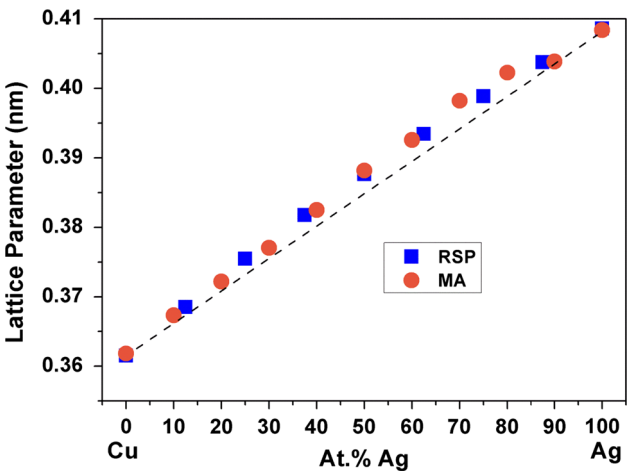

Figure 1 Variation of lattice parameter of the Cu–Ag solid solution, as a function of the Ag content, obtained by both RSP and MA methods. The lattice parameters were taken from Ref. [29] for MA powders and from Ref. [30] for RSP alloys. Note similar behavior in both the cases.

Table 1 Extension of solid solubility levels achieved by rapid solidification processing (RSP) and mechanical alloying (MA) methods

Alloy system (solvent–solute)	Equilibrium solid solubility limit (at.% solute)		Extended solubility limit (at.% solute)	
	Room temperature	Maximum	RSP	MA
Ag–Cu	0.0	14.0	100	100
Al–Mn	0.4	0.6	9.0	18.5
Al–Ti	0.0	0.75	2.0	36
Cd–Zn	3.1	4.35	35	50
Cu–Cr	0.0	0.0	4.5	50
Nb–Al	5.9	21.5	25	60
Ni–Ta	3.0	17.2	16.6	30
Ti–Si	0.0	3.5	6.0	37.5

forces and decomposition due to thermally activated jumps, described by the ratio of these two, known as the forcing parameter, γ [33]. An important general observation is that kinetic factors predominate over thermodynamic constraints in determining the formation of metastable solid solutions; this appears to be even more so in MA than RSP.

The formation of solid solutions can be explained by Hume–Rothery rules in both the cases. The atomic size factor seems to play the most important role; the electronegativity is less important. A size difference of less than about ± 15% is desired to achieve good solid solubility, noting that a smaller size factor results in a larger solubility limit. This criterion has been followed for equilibrium solubility levels and also for alloys obtained by RSP methods. However, the situation appears to be different in solid solutions obtained by MA. Figure 2a shows the variation of the maximum solid solubility of different elements in Cu obtained by MA. It is very clear from this figure that large solubilities were obtained only when the size factor was small. More importantly, the solubility achieved was small, when the size difference was large. However, when we also consider the electronegativity values and prepare a Darken–Gurry plot [34] of the systems of interest, with the electronegativity plotted against atomic size, the results are not very satisfactory (Fig. 2b). For example, elements such as Ag (100%), Al (18%), Hg (17%), Sn (9.8), and Ti (9.4%), which have extended solubility levels of over 5% in Cu, are outside the ellipse representing ± 15% atomic size difference and a ± 0.4 unit deviations of electronegativity from the value of Cu. Thus, the rules that explain the equilibrium solid solubilities may not be able to satisfactorily explain the results obtained under non-equilibrium conditions, particularly in MA powders.

By comparing the results on solid solubility extensions obtained by these two non-equilibrium processing techniques, it is clear that the solid solubility extensions achieved by MA are higher than those obtained by RSP methods. This has been explained on the basis that the maximum departure achieved in MA is much higher than that by RSP [35]. Another important microstructural difference appears to be that the grain size in the milled powders is frequently of nanometer dimensions. This certainly helps in increasing the solid solubility limits. In fact, experimental observations suggest that the solid solubility extensions achieved are the highest by MA among all the non-equilibrium processing methods. As an example, the maximum solid solubility of Fe in Cu is 0.3 at.% at room temperature under equilibrium conditions, while the extended values are 20 at.% by RSP, 35 at.% by evaporation methods, 50 at.% by sputtering, and 68 at.% by MA. Similar behavior is observed in other alloy systems as well.

Even though both RSP and MA are non-equilibrium processing methods, the solid solubility extensions achieved are different. The reasons for this difference are not very clear at present. Solid solution formation is associated with the absence of solute partition. This is relatively easy to understand in the case of RSP because of the rapid solidification rates involved during solidification. But such a situation does not exist in MA powders since they do not melt and therefore no solidification is involved. However, it is possible that segregation of solute atoms to interfaces such as grain boundaries and triple

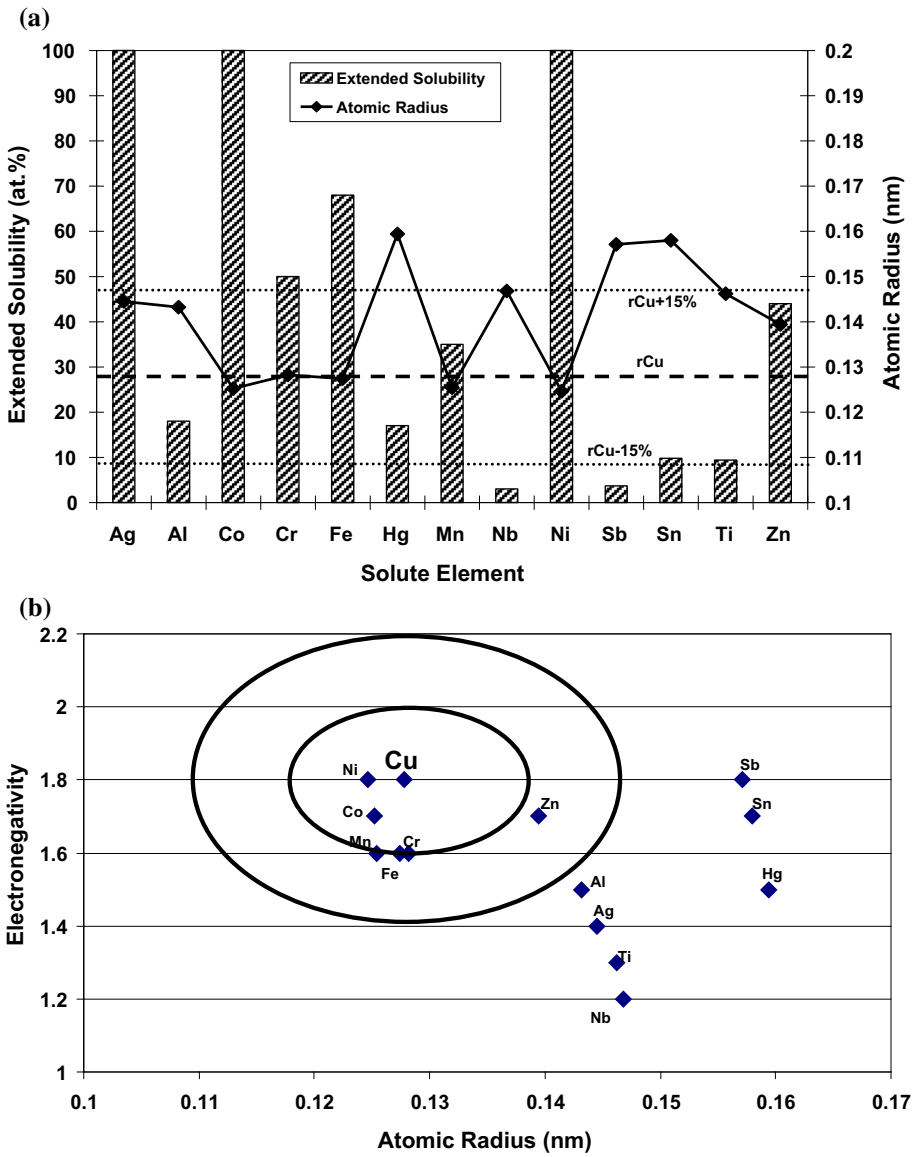

Figure 2 **a** Variation of the maximum solid solubility of different elements in Cu achieved by MA as a function of the atomic size difference. Note that elements which have a small size factor are more soluble and those that have a large size factor are less soluble. **b** Darken–Gurry plot showing the combined effect of atomic size and electronegativity on the solubility of different elements in Cu. The plot is not very satisfactory because elements that are quite soluble are present outside the outer ellipse representing an atomic size difference of ± 15% and an electronegativity difference of ± 0.4 units.

junctions in MA powders and the enhanced diffusivity due to the presence of defects could be responsible for the increased solid solubility levels in MA powders. Further work is required on this aspect.

Intermetallic phases

A number of intermetallic phases have been synthesized in different alloy systems by both RSP and MA methods. Several "missing" Hume–Rothery phases were synthesized by RSP, in addition to some novel phases, including primitive cubic phases in Te-Ag and some other alloy systems. Some high-pressure and high-temperature phases were also synthesized at atmospheric pressure and room temperature. Quasicrystalline phases (with the traditionally forbidden rotation symmetries) have also been synthesized. A partial listing of such phases may be found in the literature (see, for example, Ref. [27]).

A variety of intermetallic phases were also synthesized by MA. Even though many of the phases synthesized by MA were similar to those prepared by RSP, many other phases were also synthesized. Instead of discussing all the different phases produced by MA, let us look at some of the distinguishing features of the intermetallic phases produced by MA. These include: (1) both stable and completely novel metastable phases, (2) phases with

altered (extended) stoichiometry, and (3) phases formed due to powder contamination. A complete list (up-to-date at the time of publication) of the intermetallic phases produced by MA was presented in Refs. [23, 24].

Many equilibrium phases that are stable at room temperature were synthesized starting from blended elemental powders by MA methods. Additionally, completely novel phases, not present under equilibrium conditions in the phase diagrams, have also been synthesized. Formation of these intermetallic phases has been rationalized on the basis that they have a much lower free energy than a mixture of phases.

A number of silicide and germanide phases corresponding to the stoichiometry MSi_2 and MGe_2 (M = metal) are present under equilibrium conditions and are frequently used in the microelectronics industry. But such phases are missing in some alloy systems, and notable exceptions are $NiGe_2$ and $MnSi_2$. For example, a mixture of NiGe and Ge coexists at the Ni-66.7 at.% Ge composition under equilibrium conditions in the Ni-Ge system. MA of blended elemental powders corresponding to the Ni-66.7 at.% Ge composition resulted in the formation of the expected $NiGe_2$ phase with an orthorhombic crystal structure [36].

Another category of intermetallic phases synthesized by MA includes phases with extended stoichiometry, in addition to the extended primary solid solubility levels. It has been reported that, in comparison with the equilibrium situation, the composition range in which an intermetallic phase is produced is much wider for MA materials. Table 2 shows the situation in the Al–Mg system [37]. There are other instances where the homogeneity ranges of intermetallic phases have been extended in MA powders.

While the equilibrium NiSi phase is expected to be stable at 50 at.% Si and the $NiSi_2$ phase at 66.7 at.% Si in the Ni-Si system, these phases have formed in the MA powders at much higher Si contents. For example, the equilibrium constitution at Ni-60 at.% Si composition is expected to be a phase mixture of NiSi and $NiSi_2$; however, only the NiSi phase was present in the MA powders [38]. Similarly, at Ni-75 and 80 at.% Si compositions, a mixture of $NiSi_2$ and Si is expected to be present; but only the $NiSi_2$ phase was present at both compositions [39]. This can happen under two different situations. One is the increased homogeneity range of the NiSi and $NiSi_2$ phases to higher Si contents. But this is unlikely since these are line compounds. The second and more convincing explanation is based on the fact that some Si was lost during the milling process [40, 41]. Loss of Si during milling can occur due to possible oxidation. According to the available free energy data, the free energies for the oxidation of Si and Ni are:

$$\mathrm{Si} \rightarrow \mathrm{SiO_2}, \quad \Delta G = -853.25\ \mathrm{kJ/mol}, \text{ and}$$

$$\mathrm{Ni} \rightarrow \mathrm{NiO}, \quad \Delta G = -419.625\ \mathrm{kJ/mol}.$$

Since the oxidation of Si is so much easier (due to the lower free energy of formation of SiO_2) than that of Ni, it is possible that some Si gets oxidized during MA. This SiO_2 can react with the remaining Si and transform to SiO, which can then easily vaporize. Consequently, the Si content in the milled powder is lowered which results in formation of phases stable at lower Si contents. On the other hand, loss of Ge does not occur while milling the Ni-Ge powder blends because the free energy of formation of GeO_2 is closer to that of NiO ($Ge \rightarrow GeO_2$, $\Delta G = -518.5$ kJ/mol).

The last category of intermetallic phases in MA powders consists of phases formed due to powder contamination. As has been acknowledged by many researchers in the field of MA, powder contamination is a ubiquitous problem. Powder contamination can arise from several sources, the important ones being contaminants in the original powder, milling atmosphere, and wear and tear of the milling media. The milled powder can also be contaminated when it comes into contact with the atmosphere after opening the milling vial. While the powder purity and milling atmosphere contribute mostly the interstitial

Table 2 Extended homogeneity ranges for intermetallic phases in the Al–Mg system processed by MA [37]

Phase	Equilibrium homogeneity range (at.% Mg)	Extended homogeneity range (at.% Mg)
β-phase (Al_3Mg_2)	38.54–40.3	45–50
γ-phase ($Al_{12}Mg_{17}$)	45.0–60.5	50–70

impurities, the wear and tear of the milling media contribute substitutional impurities, mostly Fe, Cr and Ni from steel vials and W and C from WC vials/tools. The problem is exacerbated when reactive metals like Ti and Zr are milled.

Milling of blended elemental powders corresponding to the composition Ti–24Al–11Nb (at.%) results in the formation of a bcc phase, which on continued milling transforms to an fcc phase. An fcc phase also forms on milling pre-alloyed bcc Ti–24Al–11Nb powders. It was also claimed by some that this fcc phase is the disordered form of the commercially and technologically important γ-TiAl phase with tetragonal structure. Since the deformation behavior of disordered alloys is different from the behavior of ordered ones, and the former are expected to show more ductility, it was also hoped that alloys with this fcc structure will be more ductile. However, it has been noted that this fcc phase forms on milling of many different Ti-based alloys (pure Ti, different blended elemental or pre-alloyed Ti alloy powders) [42]. Therefore, doubts were cast on its nature, questioning whether it was truly the disordered form of γ-TiAl or it was a contaminant phase. This confusion was resolved by conducting a detailed structural analysis of the milled Ti alloy powder containing the fcc phase [43].

Figure 3a shows the X-ray diffraction (XRD) patterns of the pre-alloyed Ti–24Al–11Nb (at.%) powder milled for different times. The starting unmilled powder (0 h) shows the B2 ordered structure. (Because of the positions and atomic scattering factors of the elements present, the intensity of the superlattice peaks (for example, 100 at $2\theta = 27.5°$, 111 at $2\theta = 48.64°$, and 210 at $2\theta = 64.14°$) is so low that they are not seen in the XRD pattern.) The peaks are broadened after milling for 5 h due to a reduction in the crystallite size and increase in lattice strain of the milled powder. On further milling to 10.5 h, an fcc phase with $a = 0.42$ nm has formed. Figure 3b shows the Raman spectra of these powders. While the unmilled powder does not show any Raman peaks, the powder milled for 5 h shows Raman peaks at 260, 410, and 605 cm^{-1}, with a small shoulder peak at 152 cm^{-1}. The intensities of these peaks increased with increasing milling time, indicating the evolution of a new phase on milling. These peaks are at 148–153, 261^{-1}, 412, and 606 cm^{-1} indicating the presence of TiN. X-ray photoelectron spectroscopy (XPS) measurements were conducted on the as-received and milled powders to reveal the interaction, if any, between the components of the milling atmosphere (oxygen and nitrogen) and the alloy constituents. Figure 3c shows the XPS spectra of Ti 2p, Al 2p, and N 1s for the Ti–24Al–11Nb powder milled for 5 h. The Ti $2p_{3/2}$ peak appeared at 455.30 eV, close to the value expected for pure TiN (455.0–455.7 eV). Additionally, the energy separating the $2p_{1/2}$ and $2p_{3/2}$ peaks is 5.90 eV. These values are quite different from those of pure TiO_2, where the Ti $2p_{3/2}$ peak appears at 458.5–458.7 eV, and the peak separation energy is 6.15 eV. Thus, the characteristic features observed in these patterns clearly indicate the presence of TiN. The Al 2p peak appears at 73.0 and 75.5 eV. The peak at 73.0 eV corresponds to the metallic state, while the peak at 75.5 eV is ascribed to the formation of an oxide phase. The N 1s peak at 397.2 eV suggests an electron-rich state of the nitrogen atoms for a strong covalent compound such as AlN. The intensity of the N 1s peak increased with increasing milling time. These results suggest that the titanium atoms have a nitride-like interaction with the incorporated nitrogen atoms, whereas most of the Al atoms remain in the metallic state, even though some portion of them could form an oxide. Thus, the fcc phase is concluded to be TiN, formed due to nitrogenation of the titanium in the milled powder.

Figure 3 **a** X-ray diffraction patterns of the pre-alloyed Ti–24Al–11Nb (at.%) powder in the unmilled (0 h) and milled for 5 and 10.5 h. **b** Raman spectra of the Ti–24Al–11Nb (at.%) powder milled for different times. The sensitivity of the samples milled for 0 and 5 h is ×50 as high as the sample milled for10.5 h. **c** XPS spectra for Ti 2p, Al 2p, and N 1s of Ti–24Al–11Nb (at.%) powder milled for 5 h. The dotted line in Ti 2p indicates the Ti $2p_{3/2}$ peak for the powder before milling.

It should be pointed out that the last two types of phases are really neither truly metastable nor phases with altered stoichiometry. Such an altered phase constitution is achieved because of loss of silicon (or other alloying elements) from the powder blend during milling due to milling-associated problems and not fundamentally related to the actual process of MA. Therefore, if loss of these alloying elements is avoided by taking proper precautions, the equilibrium constitution only is expected to be achieved. But these are mentioned here to make researchers aware of reports where people assume that a particular phase is forming at an altered stoichiometry not

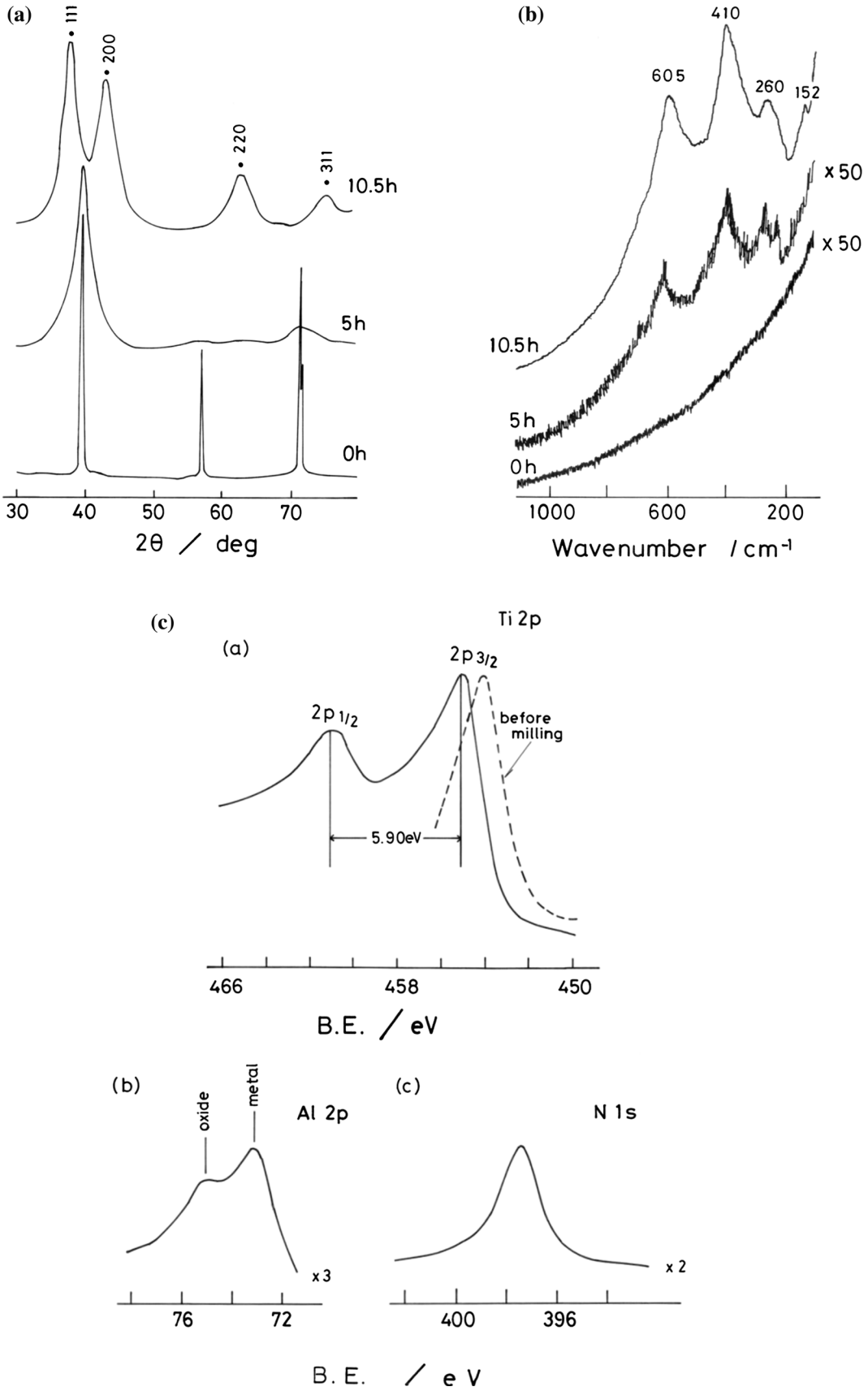
(a)
111
200
220
311
10.5h
5h
0h
30
40
50
60
70
2θ / deg
(b)
410
605
260
152
x 50
x 50
10.5h
5h
0h
1000
600
200
Wavenumber / cm-1
(c)
Ti 2p
(a)
2p3/2
2p1/2
before milling
5.90eV
466
458
450
B.E. / eV
(b)
oxide
metal
Al 2p
x 3
76
72
(c)
N 1s
x 2
400
396
B.E. / eV

because the phase is stable at different solute content but because of loss of some constituents.

Formation of contaminant phases can also be completely avoided by milling the powders in high-purity environments. For example, it was reported that a metastable fcc phase had formed on milling the pure metal Hf for long periods of time in a conventional SPEX mill. But when the powder was milled in a highly pure environment, only the equilibrium hcp phase was retained [44]. To achieve the high-purity environment, the powders were loaded into the milling vial in an evacuated and argon-filled glove box, and the lid was tightly sealed. This milling vial was then loaded into the SPEX mill which, in turn, was enclosed in a vacuum chamber that was evacuated and where the oxygen and nitrogen levels each were maintained below 1 ppm. Thus, it could be unambiguously confirmed that the fcc formed in the milled Hf powder was a contaminant phase.

Metallic glasses

Metallic glasses or amorphous alloys have been produced in a number of alloy systems by both RSP and MA methods. As highlighted earlier, the glassy phase is obtained on solidification from the liquid state (either very rapidly in the case of ribbons or more slowly in the case of bulk metallic glasses), while it is produced at near room temperature and completely in the solid state by MA methods. Additionally, it has also been reported that the amorphous phase produced by MA methods can get crystallized on continued milling, a phenomenon commonly referred to as mechanical crystallization [45–47]. The amorphous phase can also crystallize on annealing at higher temperatures, like in RSP alloys, and this can be considered as thermal crystallization. But an important difference between these two processes is that the crystalline phase is produced on continued milling of the amorphous powders obtained by MA. But in RSP alloys crystallization occurs on subsequent exposure to higher temperatures and/or pressures [48]. It has also been reported that glassy ribbons produced by RSP will also get crystallized under the action of mechanical milling [49, 50].

The most significant differences in materials produced by RSP and MA appear to be in the formation of metallic glasses. Even though metallic glasses are produced by both techniques, the systems in which glasses are formed and the composition ranges in which they are formed appear to be quite different. Additionally, the criteria for glass-forming ability and the mechanism of formation of metallic glasses also are different. We will now critically look at these two aspects.

Mechanism of glass formation

It was mentioned above that the undercooling experienced by metallic melts was responsible for the formation of metastable phases during RSP methods. This is particularly true for formation of metallic glasses. It has been shown that metallic glasses (including the bulk metallic glasses) are formed from the liquid state only when the melt was (1) solidified above the critical cooling rate for glass formation and (2) undercooled to a temperature below the glass transition temperature (T_g) for the alloy. The cooling rate and T_g are alloy (and composition) dependent. Metallic glasses were formed during solidification when these two conditions were satisfied. The required undercooling was achieved during RSP due to the rapid heat removal from the liquid when it solidified in a small section thickness. Consequently, it was possible to obtain metallic glasses only in thin foil ribbons, wires, and powder forms. However, in the case of bulk metallic glasses, significant amount of undercooling could be achieved at a low cooling rate in samples with larger cross section due to the presence of a large number of constituent elements, typically three or more.

Formation of glass (or amorphous solid, to be more accurate) has been achieved in a very large number of alloy systems by MA also. However, it is important to remember that MA is a completely solid-state process and, since a liquid phase is not involved, the ability to achieve a high solidification rate or large amount of undercooling is irrelevant when using this method. However, in the early years of research on glass formation by MA, it was argued that the powder particles melted in highly localized areas, as very high temperatures were reached due to the high rate of plastic deformation and the large amount of energy transferred to the powder particles during compression of the powder between colliding milling balls and container wall. Subsequent quenching of this small amount of liquid by heat conduction into the less deformed, and hence cooler, interior regions

of the particles resulted in the formation of the amorphous phase [51, 52]. If this is true, the mechanism for the formation of metallic glasses is very similar in both RSP and MA methods.

However, energy input calculations, temperature rise estimates, and experimental measurements suggest that the temperature rise during MA is not large enough for the powder particles to melt. It was estimated that the maximum rise in the powder temperature is about 200 K [23, 24]. Therefore, it is unlikely that this is the mechanism by which amorphous phases are obtained in MA powders. Furthermore, if this mechanism was true, the glass-forming composition ranges in MA and RSP alloys should be the same, and this is also not true.

Instead, it has been suggested that due to the high density of crystal defects introduced into the metal powders during MA, the free energy of the crystal phase is raised to a level above that of the hypothetical amorphous phase. Even though a variety of crystal defects (including dislocations, grain boundaries, stacking faults, etc.) are introduced into the powders during MA, the most significant contributions to raise the free energy arise from small grain sizes and disordering of ordered intermetallics. Amorphization takes place, if:

$$\Delta G_{\text{crystal}} + \Delta G_{\text{defects}} > \Delta G_{\text{amorphous}}$$

where ΔG represents the free energy. That is, during MA the amorphous phase gets stabilized due to the relatively low free energy of the hypothetical amorphous phase *vis-a-vis* the defected crystalline phase.

As a result of the completely different mechanisms by which the amorphous phases are formed in the RSP and MA alloys, the composition ranges in which the amorphous phases form and perhaps also the homogeneity of the phases are different in the two cases.

Glass formation composition ranges

Glass formation has been reported to occur in a variety of alloy systems by a number of non-equilibrium processing methods, but we will only compare the glass-forming composition ranges in RSP and MA alloys. Figure 4a shows the Ni–Nb equilibrium phase diagram featuring two intermetallics—Ni_3Nb and Ni_6Nb_7—in addition to the two terminal solid solutions [53]. The composition ranges in which the amorphous phase was obtained by different non-equilibrium processing techniques are shown in Fig. 4b [23]. While the glassy phase is produced in two different composition ranges by the RSP method, other methods (ion beam mixing, laser quenching, RF sputtering and MA) produce the glassy phase in a continuous and wider composition range. This is explained based on the fact that the criteria for glass formation are different in different methods. In fact, it has been possible to produce the glassy phase in the widest possible composition range by MA. Several other examples are also available in the literature [23, 24]. Table 3 clearly shows that the composition ranges for glass formation by RSP and MA methods are significantly different in different alloy systems.

Criteria for glass formation

As mentioned above, glass formation from the liquid state occurs when the critical cooling rate for glass formation is exceeded and the melt is undercooled to below T_g. Based on thermodynamic arguments for crystal nucleation, Turnbull [71] suggested that the reduced glass transition temperature, T_{rg}, defined as the ratio of T_g and the liquidus temperature of the alloy, T_ℓ, i.e., $T_{rg} = T_g/T_\ell$, should be a good indicator to evaluate the glass-forming ability of alloys. A high value of T_{rg} is easily obtained near deep eutectics (where the eutectic (liquidus) temperature is significantly lower than the individual melting temperatures of the constituent elements, while T_g is less sensitive to the composition), and therefore, researchers were able to obtain glassy alloys at such compositions determined from phase diagrams. For bulk metallic glasses (BMGs), Inoue [72] proposed that easy glass formation is possible when (1) the alloy contains at least three components, (2) a significant atomic size difference (> 12%) exists among the constituent elements, and (3) a negative heat of mixing is present among these elements. These criteria were very useful in identifying alloy systems and the appropriate composition ranges to produce BMGs.

Since 2003, a number of new criteria based on the thermal properties of the alloys and physical characteristics of the component atoms were developed, with different successes in predicting the glass-forming ability of alloys. These include the so-called α, β, γ, γ_m, δ, ϕ, etc., parameters [4, 73], listed in

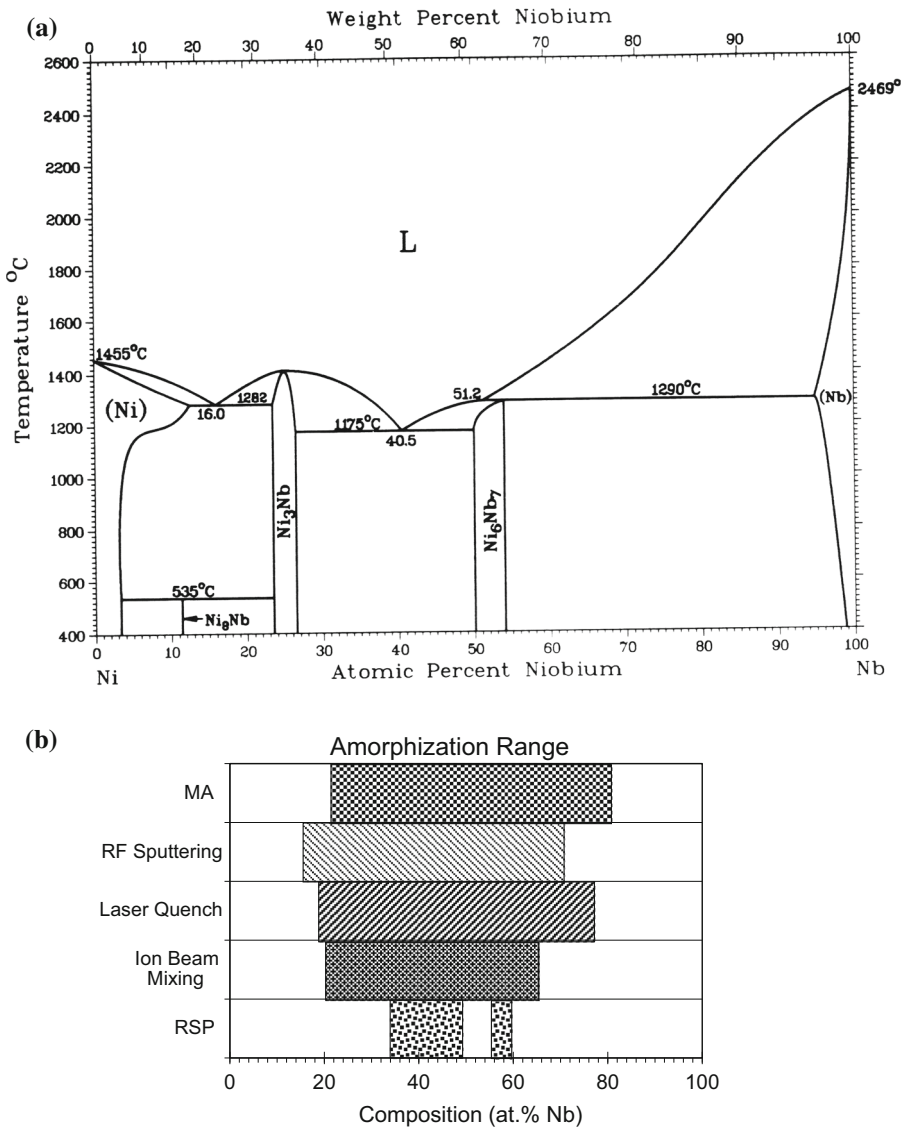

Figure 4 **a** The Ni–Nb equilibrium phase diagram showing the presence of different equilibrium phases in different composition ranges and at different temperatures [53]. **b** Composition ranges for amorphous phase formation by different non-equilibrium processing methods in the Ni–Nb system [23].

Table 3 Composition ranges for glass formation in different alloy systems by RSP and MA methods

Alloy system	Glass formation range (at.% solute)			
	By RSP	Refs.	By MA	Refs.
$Fe_{83-x}Cr_xC_{17}$	24–50 Cr	[54]	10–60 Cr	[54]
$Fe_{83-x}Mo_xC_{17}$	5–26 Mo	[54]	5–60 Mo	[54]
Ni–Nb	33.3–48 and 55–58 Nb	[55]	20–80 Nb	[56]
Ni–Ta	33.4–45 Ta	[55]	40–80 Ta	[59]
	30–60 Ta	[57]	20–90 Ta	[60]
	35–65 Ta	[58]		
Ti–Cu	30–75 Cu	[61]	10–50 Cu	[63]
	35–70 Cu	[62]	10–90 Cu	[64]
Ti–Ni	20–62 Ni	[62]	10–70 Ni	[63]
	24–46 Ni	[65]		
Zr–Co	20–52 Co	[66]	27–92 Co	[67]
Zr–Fe	20–42.5 and 88–93 Fe	[68]	30–78 Fe	[67]
Zr–Ni	20–70 Ni	[69]	27–83 Ni	[70]

Table 4. In spite of this large number of parameters, the predictability of glass formation has not improved significantly [74] and it has been difficult to exactly specify which alloy compositions would produce glassy phases and in which composition ranges. But it is important to remember that all these criteria have been developed for metallic glasses processed via the solidification route. As mentioned earlier, MA, a completely solid-state powder processing technique, is another important technique to produce amorphous alloys. But there have not been any systematic investigations on the conditions under which amorphous phases are formed by MA. Therefore, we wished to determine whether the criteria applicable to RSP studies would be applicable to the solid-state processed amorphous alloys processed by MA or other criteria need to be formulated. For this purpose, we undertook a comprehensive investigation on the glass formation behavior and stability of several Fe-based glassy alloys synthesized by MA.

Blended elemental (BE) powders corresponding to the generic composition of $Fe_{42}X_{28}Zr_{10}B_{20}$ (where the subscripts represent the composition of the alloy in atomic percentage and X = Al, Co, Ge, Mn, Ni, or Sn) were milled to determine whether they become amorphous and also the time required for their amorphization. The element X in the general alloy composition $Fe_{42}X_{28}Zr_{10}B_{20}$ was selected based on the number of intermetallics it forms with Zr under equilibrium conditions at room temperature. This number increases from 1 with Mn to 8 with Al, which provides a basis to analyze the results systematically. It was noted that amorphization had occurred in the powder blends containing Al, Ge, and Sn, but not in the blends containing Co, Mn, and Ni. This observation is rationalized on the basis that amorphization occurred in powder blends if the total number of intermetallics in the constituent binary alloy systems (X-Zr, X-Fe, and X-B) is more than 10. Further, the time required for amorphization was shorter if the total number of intermetallics was higher [75].

Table 4 Different criteria proposed to explain the glass-forming ability of bulk metallic glasses in different alloys systems [4, 73]

Criterion	Formula
T_{rg}	$T_{rg} = T_g/T_\ell$
ΔT_x	$\Delta T_x = T_x - T_g$
α	$\alpha = T_x/T_\ell$
β	$\beta = (T_x/T_g) + (T_g/T_\ell) = 1 + \alpha$
New β	New $\beta = (T_x \times T_g)/(T_\ell - T_x)^2$
γ	$\gamma = T_x/(T_g + T_\ell)$
γ_m	$\gamma_m = (2T_x - T_g)/T_\ell$
δ	$\delta = T_x/(T_\ell - T_g)$
ω	$\omega = (T_g/T_x) - [2T_g/(T_g + T_\ell)]$
ω_m	$\omega_m = (2T_x - T_g)/(T_\ell + T_x)$
ϕ	$\phi = T_{rg}\,(\Delta T_x/T_g)^{0.143}$
ς	$\varsigma = (T_g/T_\ell) + (\Delta T_x/T_x)$
K_{gl}	$K_{gl} = (T_x - T_g)/(T_\ell - T_x)$
Modified T_{rg}	Modified $T_{rg} = (T_e - T_g)/(T_\ell - T_g) \times (T_g/T_\ell)$

T_g = glass transition temperature; T_ℓ = liquidus temperature; ΔT_x = width of the supercooled liquid region; T_x = crystallization temperature; T_e = eutectic temperature

As mentioned above, amorphization in powder blends occurs when the free energy of the hypothetical amorphous phase is lower than that of the crystalline phase(s). The magnitude of energy increase in the crystalline phase due to the introduction of crystal defects is different for different types of defects. Even though increasing the dislocation density and reduction in grain size down to nanometer levels increase the free energy, the main contribution is from the presence of intermetallics in an alloy system. This is due to two important effects. First, disordering of intermetallics contributes about 15 kJ/mol to the system. Secondly, a slight change in the stoichiometry of the intermetallic increases the free energy of the system drastically. In addition, grain size reduction contributes about 5 kJ/mol. Since MA reduces the grain size to nanometer levels and also disorders the usually ordered intermetallics, the energy of the milled powders is significantly raised. In fact, it is raised to a level above that of the hypothetical amorphous phase. This condition leads to a situation when formation of the amorphous phase is favored over the crystalline phase.

In summary, even though phase diagrams are useful guidelines in choosing alloy compositions for easy glass formation by both RSP and MA methods, the features to look for appear to be quite different. It is just fortuitous that some alloy compositions can be amorphized by both the methods.

Crystallization behavior of metallic glasses

Since metallic glasses are in a non-equilibrium condition in the as-synthesized state at room temperature, they undergo crystallization on annealing at higher temperatures. Crystallization of metallic

glasses has been known to proceed in three different modes. The first is polymorphous, where the glass transforms into a crystalline state without a change in composition, i.e., a single-phase alloy is produced. The second is eutectic crystallization in which two different crystalline phases are produced simultaneously from the glassy alloy. The last one is primary crystallization in which a primary solid solution phase is produced first and the remaining glassy phase then crystallizes either in the polymorphous or eutectic mode. It was noted that the crystallization behavior of metallic glasses is very similar irrespective of whether they were produced by RSP or MA methods. However, as noted above, amorphous alloys produced by RSP or MA can be crystallized on subjecting them to milling.

Concluding remarks

We have seen above that a variety of metastable phases (solid solutions, intermetallic phases, and metallic glasses) are synthesized by both RSP and MA methods. Even though both techniques are capable of producing a variety of different phases, the solid solubility limits achieved are different, the nature of the intermetallic phases is different, and the composition ranges in which the amorphous phases produced and the criteria for glass formation seem to be quite different. These differences have been rationalized on the basis that MA is a completely solid-state process and that metastable phases are produced by the accumulation of strain energy. On the other hand, the significant amount of undercooling experienced by the melts during solidification involved in RSP methods is responsible for the formation of the metastable phases. These have been explained with specific examples.

References

[1] Suryanarayana C (ed) (1999) Non-equilibrium processing of materials. Pergamon, Oxford

[2] Suryanarayana C (1984) Metallic glasses. Bull Mater Sci 6:579–594

[3] Liebermann HH (ed) (1993) Rapidly solidified alloys: processes, structures, properties, applications. Marcel Dekker, New York

[4] Suryanarayana C, Inoue A (2018) Bulk metallic glasses, 2nd edn. CRC Press, Boca Raton

[5] Suryanarayana C, Jones H (1988) Formation and characteristics of quasicrystalline phases: a review. Int J Rapid Solidif 3:253–293

[6] Trebin HR (ed) (2003) Quasicrystals: structure and physical properties. Wiley-VCH, Weinheim

[7] Suryanarayana C (1995) Nanocrystalline materials. Int Mater Rev 40:41–64

[8] Gleiter H (2000) Nanostructured materials: basic concepts and microstructure. Acta Mater 48:1–29

[9] Suryanarayana C (2005) Recent developments in nanostructured materials. Adv Eng Mater 7:983–992

[10] Turnbull D (1981) Metastable structures in metallurgy. Metall Trans A 12:695–708

[11] Martin G, Bellon P (1997) Driven alloys. Solid State Phys 50:189–331

[12] Duwez P, Willens RH, Klement W Jr (1960) Continuous series of metastable solid solutions in Ag–Cu alloys. J Appl Phys 31:1136–1137

[13] Duwez P, Willens RH, Klement W Jr (1960) Metastable electron compound in Ag–Ge alloys. J Appl Phys 31:1137

[14] Klement W Jr, Willens RH, Duwez (1960) Non-crystalline structure in solidified gold–silicon alloys. Nature 187:869–870

[15] Duwez P (1967) Structure and properties of alloys rapidly quenched from the liquid state. Trans ASM Q 60:607–633

[16] Suryanarayana C (1991) In: Cahn RW (ed) Processing of metals and alloys. Materials science and technology: a comprehensive treatment, vol 15. VCH, Weinheim, pp 57–110

[17] Jones H (2001) A perspective on the development of rapid solidification and nonequilibrium processing and its future. Mater Sci Eng A304(306):11–19

[18] Nishiyama N, Takenaka K, Miura H, Saido N, Zeng YQ, Inoue A (2012) The world's biggest glassy alloy ever made. Intermetallics 30:19–24

[19] Suryanarayana C, Inoue A (2013) Iron-based bulk metallic glasses. Int Mater Rev 58:131–166

[20] Suryanarayana C (2002) Rapid solidification processing. In: Buschow KHJ, Cahn RW, Flemings MC, Kramer EJ, Mahajan S (eds) Encyclopedia of materials: science and technology—updates. Pergamon Press, Oxford, pp 1–10

[21] Benjamin JS (1990) Mechanical alloying: a perspective. Metal Powder Rep 45:122–127

[22] Suryanarayana C, Klassen T, Ivanov E (2011) Synthesis of nanocomposites and amorphous alloys by mechanical alloying. J Mater Sci 46:6301–6315. https://doi.org/10.1007/s10853-011-5287-0

[23] Suryanarayana C (2001) Mechanical alloying and milling. Prog Mater Sci 46:1–184
[24] Suryanarayana C (2004) Mechanical alloying and milling. Marcel Dekker, New York
[25] Takacs L (2002) Self-sustaining reactions induced by ball milling. Prog Mater Sci 47:355–414
[26] Suryanarayana C, Al-Aqeeli N (2013) Mechanically alloyed nanocomposites. Prog Mater Sci 58:383–502
[27] Anantharaman TR, Suryanarayana C (1971) A decade of quenching from the melt. J Mater Sci 6:1111–1135. https://doi.org/10.1007/BF00980610
[28] Jones H (1982) Rapid solidification of metals and alloys. The Institution of Metallurgists, London
[29] Uenishi K, Kobayashi KF, Ishihara KN, Shingu PH (1991) Formation of supersaturated solid solution in the Ag–Cu system by mechanical alloying. Mater Sci Eng A134:1342–1345
[30] Linde RK (1966) Lattice parameters of metastable silver–copper alloys. J Appl Phys 37:934
[31] Suryanarayana C, Froes FH (1990) Nanocrystalline titanium–magnesium alloys through mechanical alloying. J Mater Res 5:1880–1886
[32] Suryanarayana C, Liu JL (2012) Processing and characterization of mechanically alloyed immiscible metals. Int J Mater Res 103:1125–1129
[33] Pochet P, Tominez E, Chaffron L, Martin G (1995) Order-disorder transformation in Fe–Al under ball milling. Phys Rev B 52:4006–4016
[34] Darken LS, Gurry RW (1954) Physical chemistry of metals. McGraw-Hill, New York
[35] Froes FH, Suryanarayana C, Russell K, Li C-G (1995) Synthesis of intermetallics by mechanical alloying. Mater Sci Eng A192(193):612–623
[36] Al-Joubori A, Suryanarayana C (2015) Synthesis of metastable $NiGe_2$ by mechanical alloying. Mater Des 87:520–526
[37] Singh D, Suryanarayana C, Mertus L, Chen R-H (2003) Extended homogeneity range of intermetallic phases in mechanically alloyed Mg–Al alloys. Intermetallics 11:373–376
[38] Al-Joubori A, Suryanarayana C (2016) Synthesis of stable and metastable phases in the Ni–Si system by mechanical alloying. Powder Technol 302:8–14
[39] Suryanarayana C, Al-Joubori A (2018) Effect of initial composition on phase selection in Ni–Si powder blends processed by mechanical alloying. Mater Manufactur Proc 33:840–848
[40] Datta MK, Pabi SK, Murty BS (2000) Phase fields of nickel silicides obtained by mechanical alloying in the nanocrystalline state. J Appl Phys 87:8393–8400
[41] Zhou AJ, Zhao XB, Zhu TJ, Dasgupta T, Stiewe C, Hassdorf R, Mueller E (2010) Mechanochemical decomposition of higher manganese silicides in the ball milling process. Intermetallics 18:2051–2056
[42] Suryanarayana C (1995) Does a disordered γ-TiAl phase exist in mechanically alloyed Ti–Al powders? Intermetallics 3:153–160
[43] Sato K, Ishizaki K, Chen GH, Frefer A, Suryanarayana C, Froes FH (1993) Fine structure analysis of mechanically alloyed titanium aluminides. In: Moore JJ, Lavernia EJ, Froes FH (eds) Proceedings of the international conference on advanced synthesis of engineered structural materials, August 31–September 2, 1992. ASM International, Materials Park, pp 221–225
[44] Seelam UMR, Barkhordarian G, Suryanarayana C (2009) Is there a hexagonal close-packed (hcp) → face-centered cubic (fcc) allotropic transformation in mechanically milled Group IVB elements? J Mater Res 24:3454–3461
[45] Patil U, Hong SJ, Suryanarayana C (2005) An unusual phase transformation during mechanical alloying of an Fe-based bulk metallic glass composition. J Alloy Compd 389:121–126
[46] Sharma S, Suryanarayana C (2007) Mechanical crystallization of Fe-based amorphous alloys. J Appl Phys 102:083544-1–083544-7
[47] Sharma S, Suryanarayana C (2008) Effect of carbon addition on the glass-forming ability of mechanically alloyed Fe-based alloys. J Appl Phys 103:013504-1–013504-5
[48] Suryanarayana C, Wang WK, Iwasaki H, Masumoto T (1980) High pressure synthesis of A15 Nb_3Si phase from amorphous titanium-silicon alloys. Solid State Commun 34:861–863
[49] Trudeau ML, Schulz R, Dussault D, Van Neste A (1990) Structural changes during high-energy ball milling of iron-based amorphous alloys: is high-energy ball milling equivalent to a thermal process? Phys Rev Lett 64:99–102
[50] Guo FQ, Lu K (1997) Ball-milling-induced crystallization and ball-milling effect on thermal crystallization kinetics in an amorphous FeMoSiB alloy. Metall Mater Trans A28:1123–1131
[51] Yermakov AE, Yurchikov EE, Barinov VA (1981) The magnetic properties of amorphous Y–Co alloy powders obtained by mechanical comminution. Phys Met Metallogr 52(6):50–58
[52] Yermakov AE, Barinov VA, Yurchikov EE (1982) The change in the magnetic properties of Gd–Co alloy powders during their amorphization by comminution. Phys Met Metallogr 54(5):90–96

[53] Massalski TB, Okamoto H, Subramanian PR, Kacprzak L (eds) (1990) Binary alloy phase diagrams, 2nd edn. ASM International, Materials Park

[54] Omuro K, Miura H (1995) Amorphization of mechanically alloyed Fe–C and Fe–N materials with additive elements and their concentration dependence. Mater Sci Forum 179–181:273–280

[55] Ruhl RC, Giessen BC, Cohen M, Grant NJ (1967) New microcrystalline phases in the Nb–Ni and Ta–Ni systems. Acta Metall 15:1693–1702

[56] Petzoldt F (1988) Synthesis and process characterization of mechanically alloyed amorphous Ni–Nb powders. J Less Common Metals 140:85–92

[57] Giessen BC, Madhava M, Polk DE, Vander Sande J (1976) Refractory amorphous inter-transition metal alloys. Mater Sci Eng 23:145–150

[58] Rohr L, Reimann P, Richmond T, Güntherodt HJ (1991) Refractory metallic glasses. Mater Sci Eng A133:715–717

[59] Lee PY, Chen TR (1994) Formation of amorphous Ni–Ta alloy powders by mechanical alloying. J Mater Sci Lett 13:888–890

[60] Lee PY, Yang JL, Lin HM (1998) Amorphization behavior in mechanically alloyed Ni–Ta powders. J Mater Sci 33:235–239. https://doi.org/10.1023/A:1004334805505

[61] Sakata M, Cowlam N, Davies HA (1982) In: Masumoto T, Suzuki K (eds) Proceedings of the international conference on rapidly quenched metals IV (RQ4). Japan Inst Metals, Sendai, pp 327–330

[62] Rabinkin A, Liebermann H, Pounds S, Taylor T, Reidinger F, Lui SC (1991) Amorphous TiZr; base Metglas brazing filler metals. Scripta Metall Mater 25:399–404

[63] Murty BS, Ranganathan S, Mohan Rao M (1992) Solid state amorphization in binary Ti–Ni, Ti–Cu and ternary Ti–Ni–Cu system by mechanical alloying. Mater Sci Eng A149:231–240

[64] Krauss W, Politis C, Weimar P (1988) Preparation and compaction of mechanically alloyed amorphous materials. Metal Powder Rep 43:231–238

[65] Buschow KHJ (1984) Stability and electrical transport properties of amorphous $Ti_{1-x}Ni_x$ alloys. J Phys F Metal Phys 13:563–571

[66] Altounian Z, Shank RJ, Strom-Olsen JO (1985) Crystallization characteristics of Co–Zr metallic glasses from $Co_{52}Zr_{48}$ to $Co_{20}Zr_{80}$. J Appl Phys 58:1192–1195

[67] Eckert J, Schultz L, Urban K (1988) Glass-forming ranges in transition metal-Zr alloys prepared by mechanical alloying. J Less Common Metals 145:283–291

[68] Altounian Z, Volkert CA, Strom-Olsen JO (1985) Crystallization characteristics of Fe–Zr metallic glasses from $Fe_{43}Zr_{57}$ to $Fe_{20}Zr_{80}$. J Appl Phys 57:1777–1782

[69] Altounian Z, Guo-hua T, Strom-Olsen JO (1983) Crystallization characteristics of Ni–Zr metallic glasses from $Ni_{20}Zr_{80}$ to $Ni_{70}Zr_{30}$. J Appl Phys 54:3111–3116

[70] Eckert J, Schultz L, Hellstern E, Urban K (1988) Glass-forming range in mechanically alloyed Ni–Zr and the influence of the milling intensity. J Appl Phys 64:3224–3228

[71] Turnbull D (1969) Under what conditions can a glass be formed? Contemp Phys 10:473–488

[72] Inoue A (2000) Stabilization of metallic supercooled liquid and bulk amorphous alloys. Acta Mater 48:279–306

[73] Bazlov AI, Tsarkov AA, Ketov SV, Suryanarayana C, Louzguine-Luzgin DV (2018) Effect of multiple alloying elements on the glass-forming ability, thermal stability, and crystallization behavior of Zr-based alloys. Metall Mater Trans A49:644–651

[74] Suryanarayana C, Seki I, Inoue A (2009) A critical analysis of the glass-forming ability of alloys. J Non Cryst Solids 355:355–360

[75] Sharma S, Vaidyanathan R, Suryanarayana C (2007) Criterion for predicting the glass-forming ability of alloys. Appl Phys Lett 90:111915